Phase diagram of C_{60} from *ab initio* intermolecular potential

A. L. C. Ferreira
Departmento de Física, Universidade de Aveiro, 3810-193 Aveiro, Portugal

J. M. Pacheco
Departmento de Física da Universidade, 3004-516 Coimbra, Portugal

J. P. Prates-Ramalho
Departmento de Química, Universidade de Évora 7001 Évora codex, Portugal

(Received 6 December 1999; accepted 14 April 2000)

Recently a new intermolecular potential for C_{60} was derived from *ab initio* calculations. Using this new interaction potential we numerically study the phase diagram of fullerite. Several numerical techniques are used in order to ascertain the correctness of the results. We predict that C_{60} can be found in the liquid state for densities between 0.468 and 0.845 nm^{-3} and temperatures between 1881 and 2012 K. © *2000 American Institute of Physics.* [S0021-9606(00)51126-X]

I. INTRODUCTION

The behavior of fullerite-C_{60} at densities and temperatures where a solid phase coexists with fluid phases remains an open problem. On the theoretical side, the pioneering works of Hagen *et al.*[1] and Cheng *et al.*[2] were in conflict regarding the question of the stability of the liquid phase. Experiments have been also unable to provide an unambiguous answer to this question so far. From the technological point of view, the existence of liquid C_{60} would be very interesting regarding its application as a lubricant. The interval of temperature and densities where the liquid phase may eventually be stable being possibly quite small, a good experimental control of pressure and temperature is needed to search for the liquid phase. Furthermore, it is possible that the region of liquid stability occurs at temperatures where the C_{60} molecule could start to polymerize.[3]

Previous theoretical calculations start with a phenomenological interaction potential proposed by Girifalco. The Girifalco potential is anomalous as compared to the Lennard-Jones potential because it is deeper and the attraction range is smaller and steeper. Ashcroft[4] argued that the short-range character of the attraction in the Girifalco potential could lead to the metastability of the liquid phase of C_{60}. The role of the interaction range was further studied in the context of the hard sphere Yukawa fluid,[5] where it was found that for sufficiently short interaction ranges the system has no stable liquid phase.

Hagen *et al.* used the Gibbs ensemble method[6] to compute the liquid-vapor coexistence line and Gibbs-Duhem integration[7] to compute the solid-fluid coexistence line and found that the liquid phase of C_{60} is metastable. On the other hand, Cheng *et al.*, using integral equation methods (HMSA, hypernetted mean spherical approximation) and a freezing entropic criterion due to Giaquinta and co-workers,[8] found the triple point at a temperature $T_{TP}=1774$ K and density $\rho_T=0.944$ nm^{-3} and a critical point at temperature $T_C=2050$ K and density $\rho_c=0.56$ nm^{-3}. The critical temperature found by Hagen *et al.* was considerably lower, $T_C=1798\pm10$ K. More recent studies for the Girifalco potential using the MHNC approximation (modified hypernetted chain),[9] together with the entropic criterion for the freezing, gave a stable liquid phase with $T_{TP}=1620$ K and $\rho_{TP}=1$ nm^{-3} and $T_C=1920$ K, $\rho_c=0.6$ nm^{-3}. Yet another method, HRT (hierarchical reference theory), was applied to the Girifalco potential,[10] giving both T_C and T_{TP} at a much higher value, $T_C=2138$ K, $\rho_C=0.5$ nm^{-3}, $T_{TP}=1979$ K and $\rho_{TP}=0.848$ nm^{-3}. It is quite interesting to note that integral equation methods give results for the binodal and the freezing line of the Lennard-Jones[9] system in good agreement with results obtained from free energy calculations.[11]

An important issue is the adequacy of the Girifalco's potential to reproduce the properties of C_{60}. A different but related interaction potential was proposed by Broughton and co-workers[12] which is a shell model in which the radius of each molecule is allowed to be a dynamical variable. Using isothermal isobaric molecular dynamics and free-energy calculations, the authors found, in agreement with Hagen *et al.*, no triple point. Recently, two of us[13] have proposed an *ab initio* interaction potential that is able to reproduce more accurately the experimental pressure-volume isotherm data at high pressures (up to 20 GPa). This new interaction potential is considerably softer at short distances than the Girifalco potential.

The purpose of the present work is to determine accurately the phase diagram of C_{60} making use of this new interaction potential. Due to computer time limitations, we have not included in the calculations the three-body AT (Axilrod-Teller) interaction term also known for the C_{60} system.[13] Being mostly repulsive, the AT term will shift the two-body potential phase diagram to lower temperatures. The liquid-vapor coexistence line was obtained by us both from Gibbs ensemble simulations and from the computation of relative free energies all the way from the vapor phase to the liquid phase crossing the thermodynamically unstable two-phase region. We made use of a recently developed method based on the generalization of multiple histograms to volume and temperature extrapolations (GMH) rather than temperature extrapolations alone.[14] For the solid-fluid coex-

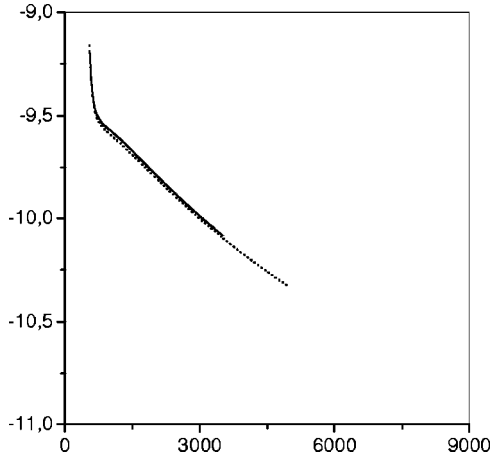

FIG. 1. Helmholtz free energy $\beta F(T,V)/N$, as a function of volume per particle at $T=2000$ K for system sizes $N=108$ (solid line), 256 (dotted line) and $N=500$ (dashed line). The results for $N=108$ include data up to 8500 cm^3/mol and data for $N=256$ and $N=500$ include data up to 5000 cm^3/mol only.

istence we have first computed absolute free energies of the solid and of the fluid phase at a given density and temperature and then we use the GMH method to compute differences in free energies to other thermodynamic states. The coexistence curves are obtained from the free-energy curves by the application of the double tangent construction. The absolute free-energy calculations allow us to avoid possible ergodicity problems expected for simulations done in the two-phase region where the crystal coexists with the fluid.

II. FREE-ENERGY CALCULATIONS AND SIMULATION DETAILS

The expression for the interaction potential used in the present work can be found in Eq. (2) and Table I of Ref. 13. We studied systems of $N=108$, $N=256$ and $N=500$ particles and we made various series of canonical ensemble (NVT) simulations. Each series is done at a given temperature. For the system with 108 particles we made two series of simulations, one at 2000 K and another at 1800 K. For 256 particles we made a series of simulations at 2000 K and for $N=500$ the corresponding series was made at 1900 K.

The series of simulations for the largest systems ($N=256$ and $N=500$) covers specific volumes from 425 cm^3/mol up to volumes of 5000 cm^3/mol. For the smallest system specific volumes as large as 8500 cm^3/mol were considered. Each series of simulations includes around 80 simulations. The simulations are done in a cubic box and the particle positions are initially in a face centered cubic (fcc) lattice. In a typical run we made 50 000 MCS/N (Monte Carlo steps per particle) for equilibration and we made measures for another 50 000 MCS/N. The measurements were saved into a file, therefore being available for later analysis. We have always used a cutoff radius equal to half the length of the simulation box. In all our calculations we have corrected the results, including standard long-range corrections.[15] We combine each pair of closest volumes simulations in a series using the GMH method that allow us to compute Helmholtz free energies at different volumes and temperatures relative to some thermodynamic state. For the application of the GMH method we measure the volume derivatives of the internal energy up to fifth order.[14] The main quantity we compute is $\beta F^C(T,V)-\beta_S F^C(T_S,V_R)$, where T_S is the simulation temperature, V_R is the volume of one of the simulations in the series and $F^C(T,V)$ is the configurational part of the Helmholtz free energy.

TABLE I. Values of $\beta_S F^{\rm exc}(T_S,V_R)/N$ at $V_R=430$ cm^3/mol for different system sizes and different simulation temperatures.

N	T_S (K)	$\beta_S F^{\rm exc}(T_S,V_R)/N$ without corrections	$\beta_S F^{\rm exc}(T_S,V_R)/N$ with corrections
108	1800	−2.104	−2.2774
500	1900	−1.725	−1.7574
108	2000	−1.148	−1.3039
256	2000	−1.241	−1.3022
500	2000	−1.268	−1.2986

The excess Helmholtz free-energy relative to the ideal gas is defined by

$$\beta F^{\rm exc}(T,V)=\beta[F(T,V)-F^{\rm id}(T,V)] = \beta F^C(T,V)-N(\ln\rho-1), \quad (1)$$

where $F^{\rm id}(T,V)$ is the ideal gas free energy. The above equation can be rewritten as

$$\beta F^{\rm exc}(T,V)=\beta_S F^{\rm exc}(T_S,V_R) + [\beta F^C(T,V)-\beta_S F^C(T_S,V_R)]+N\ln\frac{\rho_R}{\rho}. \quad (2)$$

The quantity $\beta F^C(T,V)-\beta_S F^C(T_S,V_R)$ is directly measured from the simulations and given by the GMH method. Thus we need to compute $\beta_S F^{\rm exc}(T_S,V_R)$ for a suitable reference state. To obtain the fluid excess free energy we would like to use as a reference thermodynamic point a system with very small density such that the excess free energy relative to the ideal gas is small. Considering only the second virial correction we obtain $\beta_S F^{\rm exc}(T_S,V_R)=B_2(T_S)\rho_R$. The computation of the second virial coefficient for $T=2000$ K gives $B_2=-2.557\,81$ nm^3 and for $T=1900$ K we obtain $B_2=-2.913\,98$ nm^3.

The Gibbs ensemble simulations were performed for a system of 500 particles. As with the GMH simulations, standard long-range corrections, although small, were always considered, as well as the range of the interaction, which has been taken as half the length of the simulation boxes. For each simulation we have made 50 000 MCS/N for equilibration and another 70 000 MCS/N for averages.

III. RESULTS AND DISCUSSION

In Fig. 1 we show the absolute configurational Helmholtz free-energy value $\beta F^C(T,V)/N=\beta F^{\rm exc}(T,V)/N+\ln\rho-1$ for each of the three system sizes studied and for $T=2000$ K. Results for $N=108$ include data up to 8500 cm^3/mol, whereas results for $N=256$ and $N=500$ include data up to 5000 cm^3/mol. The absolute value of the free energy for the system with biggest volume (the reference point) is computed from the second virial coeficient. The

three curves are nearly coincident in spite of the fact that the reference point for $N=108$ is taken at a larger volume than the one taken for $N=256$ and $N=500$. This means that the second virial coefficient is the most important correction to the ideal gas limit already for systems with specific volumes equal to 5000 cm^3/mol. Furthermore, one should note that the results for $N=500$ are obtained from simulations at $T_S=1900$ K and from the value of B_2 at this temperature.

To compute the absolute free energy of the solid we use $V_R=430$ cm^3/mol as the thermodynamic reference point and we compute $\beta_S F^{\rm exc}(T_S,V_R)$ by coupling the system harmonically to a lattice. Following the method given by Frenkel and Smit[16] we measure $\beta_S \Delta f_{\rm CM}=\beta_S[F^C_{\rm CM}(T_S,V_R)-F^{C,{\rm Ein}}_{\rm CM}(T_S,V_R)]/N$, where $F^C_{\rm CM}(T_S,V_R)$ is the configurational Helmholtz free energy of the system with constrained center of mass motion at T_S and V_R and $F^{C,{\rm Ein}}_{\rm CM}(T_S,V_R)/N$ is the configurational Helmholtz free energy of the corresponding Einstein solid with constrained center of mass motion. The modified configurational energy we use is given by

$$\tilde{U}(\{\boldsymbol{r}_i\})=U(\{\boldsymbol{r}_i^0\})+(1-\lambda)[U(\{\boldsymbol{r}_i\})-U(\{\boldsymbol{r}_i^0\})]+\lambda\alpha\sum_{i=1}^{N}(\boldsymbol{r}_i-\boldsymbol{r}_i^0)^2, \tag{3}$$

where $\{\boldsymbol{r}_i^0\}$ are the sites of the underlying fcc lattice and $U(\{\boldsymbol{r}_i\})$ is the internal energy of the system when the particles are in the coordinate configuration $\{\boldsymbol{r}_i\}$. Note that when $\lambda=1$ we recover the Einstein solid limit and when $\lambda=0$ we recover the unmodified configurational energy.

The quantity $\beta_S F^{C,{\rm Ein}}_{\rm CM}(T_S,V_R)/N$ is computed from[16]

$$\beta_S F^{C,{\rm Ein}}_{\rm CM}(T_S,V_R)/N=-\frac{3(N-1)}{2N}\ln\frac{\pi}{\alpha\beta_S}+\frac{3}{2N}\ln N+\beta_S U(\{\boldsymbol{r}_i^0\})/N. \tag{4}$$

In all our calculations we found convenient to choose[16] $\alpha=1$ eV/Å^2. The results for the excess value $\beta_S F^{\rm exc}(T_S,V_R)$ are obtained from

$$\beta_S F^{\rm exc}(T_S,V_R)/N=\beta_S\Delta f_{\rm CM}+\beta_S F^{C,{\rm Ein}}_{\rm CM}(T_S,V_R)/N-\frac{\ln V_R}{N}-(\ln\rho_R-1). \tag{5}$$

The term $\ln V_R$ is the increase in the Helmholtz free energy due to the constraint on the center of mass position and must be subtracted.

For each system size we made 11 simulations at equally spaced values of λ in the interval $[0,1]$ at T_S and $V_R=430$ cm^3/mol. We neglected the initial 50 000 MCS/N and made measurements in the following 100 000 MCS/N. From these simulations we obtain $\beta_S\Delta f_{\rm CM}$. Using Eqs. (2) and (5) we are able to compute the Helmholtz free energy of the solid at a given temperature and volume. It is important to include the correction due to the finite cutoff radius used in the simulations when calculating $\beta_S U(\{\boldsymbol{r}_i^0\})/N$. In Table I we show the measured values for $\beta_S F^{\rm exc}(T_S,V_R)/N$ with and without the long-range correction.

In Fig. 2 we plot Helmholtz free energy of the solid as a function of the volume per particle for $T=2000$ K. Almost no finite size effects are seen except deep inside the thermodynamically unstable region.

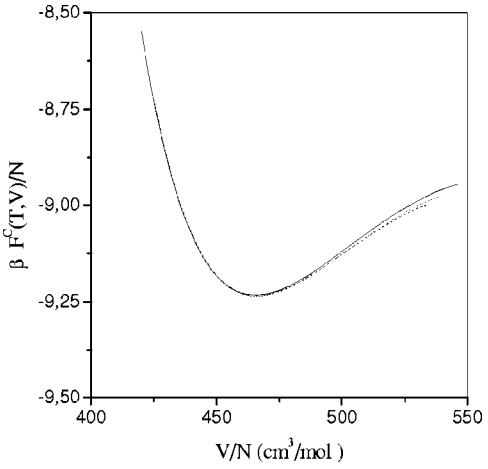

FIG. 2. Helmholtz free energy of the solid $\beta F(T,V)/N$, as a function of the volume per particle at $T=2000$ K for system sizes $N=108$ (solid line), 256 (dotted line) and $N=500$ (dashed line).

A. Liquid-vapor coexistence

For the study of the liquid-vapor coexistence we used directly the values of $\beta F^C(T,V)-\beta_S F^C(T_S,V_R)$. We show in Fig. 3 the quantity $\beta F^C(T,V)/N-\beta_S F^C(T_S,V_R)/N$ for a system size $N=256$, $T=1950$ K, $V_R=540$ cm^3/mol and $T_S=2000$ K as a function of the specific volume. We also plot the two tangent straight lines at the coexisting specific volumes that have a common slope and that coincide with the straight line joining the two tangent points (double tangent construction). The symmetric value of this common slope gives the pressure at coexistence, $P_{L-V}(T)$.

In Fig. 4 we show the liquid-vapor binodal line determined by the free-energy calculations together with Gibbs ensemble results. The two methods agree quite well. The finite size effects observed are also not very pronounced.

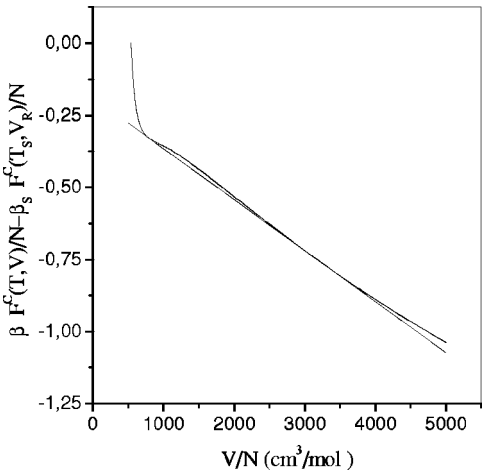

FIG. 3. The quantity $\beta F^C(T,V)/N-\beta_S F^C(T_S,V_R)/N$ for a system size $N=256$, $T=1950$ K, $T_S=2000$ K and $V_R=540$ cm^3/mol as a function of the specific volume.

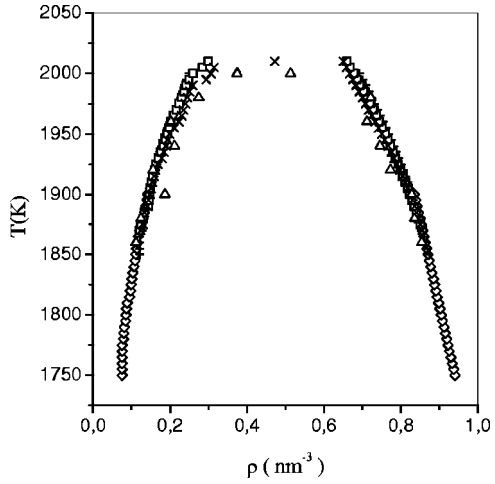

FIG. 4. Liquid-vapor phase coexistence in the temperature density plane. Results for systems of sizes $N=108$ ($\diamond$, $T_S=1800$ K and $+$, $T_S=2000$ K), $N=256$ ($\square$), $N=500$ ($\times$) and for the Gibbs ensemble ($\triangle$) are shown.

The critical temperature and densities were estimated by an analysis of the results in the vicinity of the critical point. The critical parameters were obtained from a fit to the law of rectilinear diameters

$$\frac{\rho_l+\rho_v}{2}=\rho_c+A(T-T_C) \tag{6}$$

and the scaling law

$$\rho_l-\rho_v=B(T_C-T)^{\beta}, \tag{7}$$

where the critical exponent β was taken as 0.32. ρ_l and ρ_v stand for the liquid and vapor densities, respectively, and A and B are fitting parameters. From this analysis we obtained $T_C=2011.7\pm1.1$ K and $\rho_c=0.4676\pm0.0007$ nm^{-3}.

In Figs. 5–7 we present results for the coexistence values of the internal energy [$U_L(T)$ and $U_V(T)$], the coexistence pressure [$P_{L-V}(T)$] and the excess Helmholtz free energy ($\beta F_L^{\mathrm{exc}}/N$ and $\beta F_V^{\mathrm{exc}}/N$).

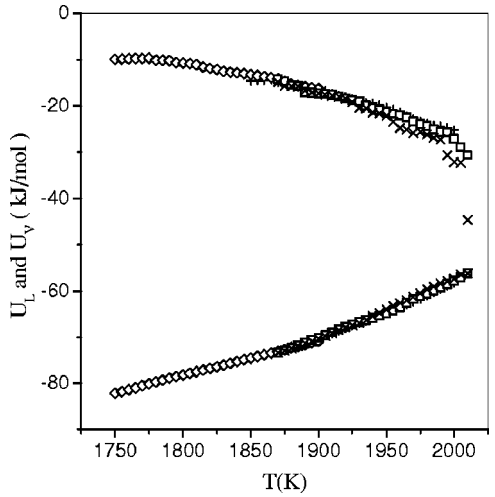

FIG. 5. Liquid (lower curve) and vapor (upper curve) internal energies at coexistence. Same notation as in Fig. 4.

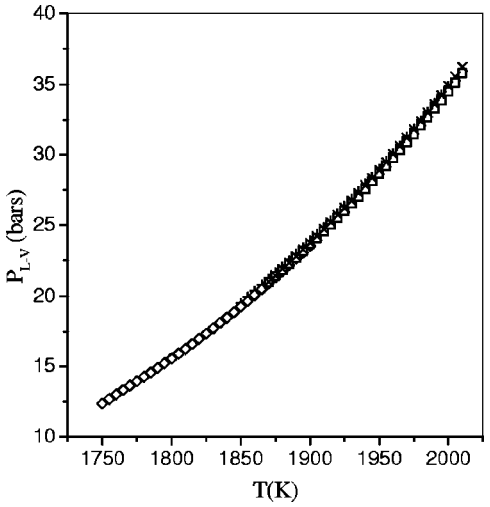

FIG. 6. Liquid-vapor coexistence pressure as a function of temperature. Same notation as in Fig. 4.

B. Solid-fluid coexistence

To compute the solid-fluid coexistence properties we have first determined the absolute Helmholtz free energies of the solid and of the fluid phases. In this way we avoid the use of the simulations in the thermodynamically unstable region between the solid and the fluid that could, in principle, give us the relative free energy of the two phases. In that region ergodicity problems are expected that could spoil the results. These ergodicity problems are not present in the liquid-vapor coexistence region, as can be seen by the good agreement of the results provided by the GMH method and the Gibbs ensemble method.

In Fig. 8 we show the solid and the fluid absolute values of $\beta F^C(T,V)/N$ for a system of 500 particles at $T=2000$ K.

The solid-fluid coexistence pressure, P_{S-F}, is plotted as a function of temperature in Fig. 9. In the same figure we plot the data for P_{L-V}, the pressure at the liquid-vapor coexistence, as a line. The triple point is clearly seen as a change of slope in the $P_{S-F}(T)$ curve. The data for tempera-

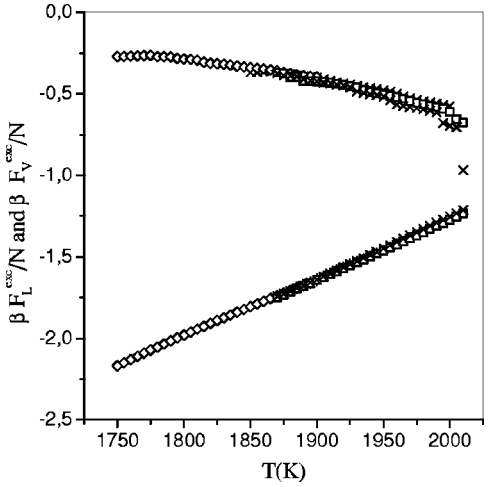

FIG. 7. Liquid excess Helmholtz free energy (lower curve), $\beta F_L^{\mathrm{exc}}/N$ and vapor excess Helmholtz free energy (upper curve), $\beta F_V^{\mathrm{exc}}/N$ at coexistence as a function of temperature. Same notation as in Fig. 4.

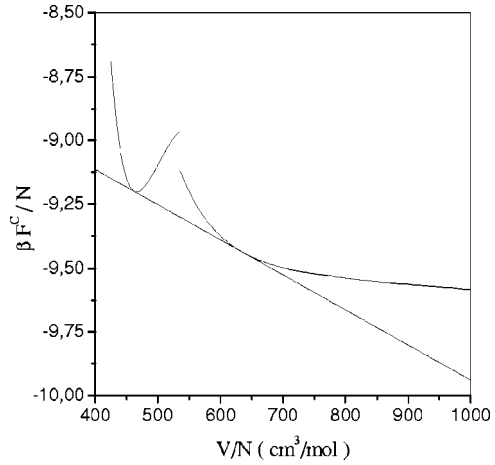

FIG. 8. $\beta F^C(T,V)/N$ at 2000 K for the fluid phase and the solid phase as a function of the volume per particle for a system of $N=500$ particles.

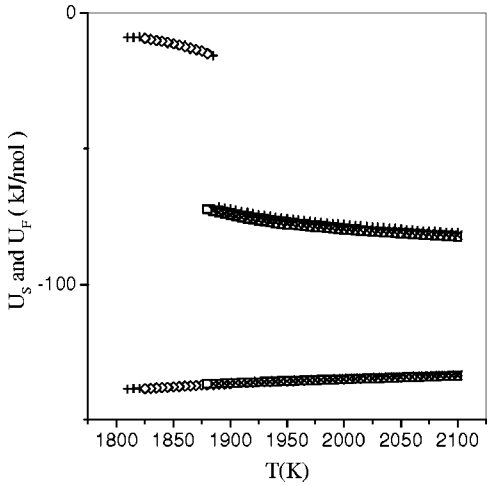

FIG. 10. Solid (lower curve) and fluid (upper curve) internal energies at coexistence as a function of temperature. Same notation as in Fig. 4.

tures smaller than 1800 K that correspond to fluid densities smaller than 0.12 nm^{-3} are obtained assuming equilibria with an ideal gas with second virial corrections.

In Fig. 10 we plot the coexistence values of $U_S(T)$ and $U_F(T)$. In Fig. 11 we also show the coexistence values of the excess Helmholtz free energy for the solid, $F_S^{\text{exc}}(T)$ and for the fluid $F_F^{\text{exc}}(T)$.

In Fig. 12 we show, in the density-temperature plane, the combined results for the solid-fluid coexistence line together with results for the liquid-vapor coexistence line. The results for the solid-fluid coexistence shown for $N=256$ and $N=500$ with $\rho \leqslant 0.12$ nm^{-3} were obtained assuming that the solid is in equilibrium with an ideal gas with a second virial correction. We obtain a triple point temperature $T_{TP}=1881.2$ K and density $\rho_{TP}=0.8447$ nm^{-3}. Analysis of Fig. 12 shows that a stable liquid phase exists in a small region of the phase diagram of fullerite. The limiting temperature and number density intervals which define this phase are 1881–2012 K and 0.468–0.845 nm^{-3}, respectively. The results obtained with this new potential support the conclusions reached by Cheng *et al.* on the basis of the phenomenological Girifalco potential in what concerns the existence of a stable liquid phase. However, the values obtained for the critical and triple-point temperatures are different, reflecting the different physical content of the interfullerene interaction used.

IV. CONCLUDING REMARKS

We studied the phase diagram of C_{60} in the region where the face centered cubic solid phase is in equilibrium with fluid phases. We made use of a recently obtained *ab initio* interaction potential for C_{60} molecules together with a new method, the GMH method, that allows us to compute Helmholtz free-energy differences relative to some thermodynamic state. These relative free energies were used to directly find the liquid-vapor coexistence properties. The results obtained were found to be in close agreement with Gibbs ensemble simulations. To investigate the solid-fluid coexistence properties we first obtained absolute free-energy values of the solid and of the fluid phases for a given thermodynamic reference state. The computation of absolute free

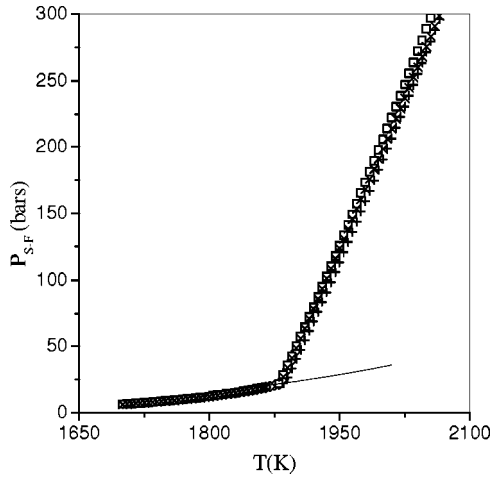

FIG. 9. Solid-fluid coexistence pressure as a function of temperature. Same notation as in Fig. 4.

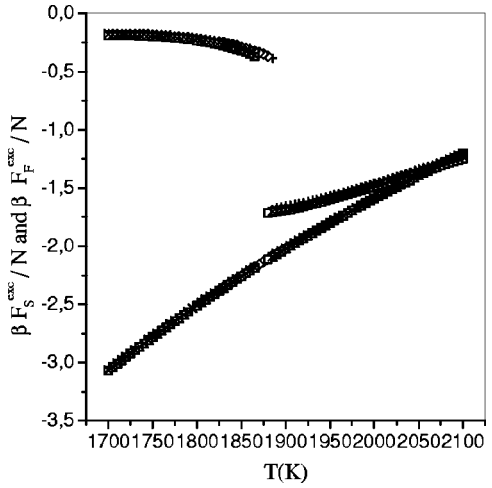

FIG. 11. Solid excess Helmholtz free energy (lower curve), $\beta F_S^{\text{exc}}/N$ and fluid excess Helmholtz free energy (upper curve), $\beta F_F^{\text{exc}}/N$ at coexistence as a function of temperature. Same notation as in Fig. 4.

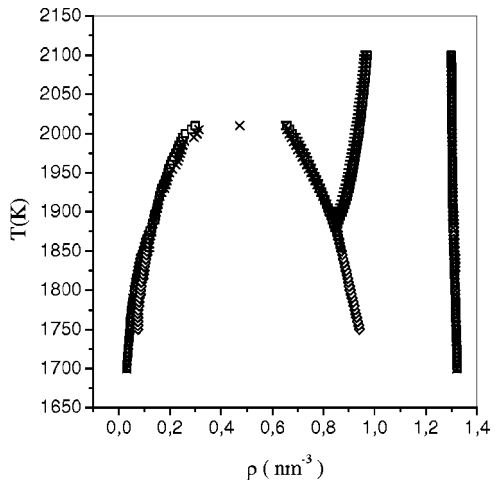

FIG. 12. Phase diagram in the density-temperature plane. Same notation as in Fig. 4.

energies is required because simulations done in the thermodynamically unstable solid-fluid coexistence region are not ergodic. In this region the system becomes trapped in metastable disordered solid configurations. To measure the absolute free energy of the solid phase we construct a thermodynamic path connecting the solid to an Einstein solid. The results show a very small finite size dependence. For the fluid phase we found that the inclusion of the second virial correction to the ideal gas is enough to get reliable absolute free energies for the biggest simulated specific volumes. We have obtained several thermodynamic coexistence properties. The results show that a liquid phase is stable for temperatures $T_{TP} \leqslant T \leqslant T_C$ with $T_C = 2011.7 \pm 1.1$ K, $T_{TP} = 1881.2 \pm 0.1$ K and for densities $\rho_C \leqslant \rho \leqslant \rho_{TP}$, with $\rho_c = 0.4676 \pm 0.0007$ nm^{-3} and $\rho_{TP} = 0.8447 \pm 0.0003$ nm^{-3}.

As pointed out before, it would be relevant to assess the role of three-body forces in the definition of the phase diagram of fullerite. Because of the peculiar character of the interfullerene interaction, the three-body forces are expected to induce sizable changes on the position of the critical and triple points. However, we do not expect any changes in the overall topology of the coexistence curves in the phase diagram. Work along these lines is in progress.

ACKNOWLEDGMENT

The authors acknowledge financial support from the Ministry of Science and Technology under Contract Nos. PRAXIS/2/2.1/299/94, PRAXIS/2/2.2/FIS/302/94 and PRAXIS/C/FIS/10019/98.

[1] M. H. J. Hagen *et al.*, Nature (London) **365**, 425 (1993).
[2] A. Cheng, M. L. Klein, and C. Caccamo, Phys. Rev. Lett. **71**, 1200 (1993).
[3] S. D. Leifer *et al.*, Phys. Rev. B **51**, 9973 (1995).
[4] N. W. Ashcroft, Nature (London) **365**, 387 (1993).
[5] E. Lomba and N. G. Almarza, J. Chem. Phys. **100**, 8367 (1994).
[6] A. Z. Panagiotopoulos, Mol. Simul. **9**, 1 (1992).
[7] D. A. Kofke, J. Chem. Phys. **98**, 4149 (1993).
[8] P. V. Giaquinta and G. Giunta, Physica A **187A**, 145 (1992); P. V. Giaquinta, G. Giunta, and S. Prestipino Giarrita, Phys. Rev. A **45**, R6966 (1992).
[9] C. Caccamo, Phys. Rev. B **51**, 3387 (1995).
[10] M. Tau, A. Parola, D. Pini, and L. Reatto, Phys. Rev. E **52**, 2644 (1995).
[11] J.-P. Hansen and L. Verlet, Phys. Rev. **184**, 151 (1969).
[12] J. Q. Broughton, J. V. Lill, and J. K. Johnson, Phys. Rev. B **55**, 2808 (1997).
[13] J. M. Pacheco and J. P. Prates Ramalho, Phys. Rev. Lett. **79**, 3873 (1997).
[14] A. L. Ferreira and M. A. Barroso, Phys. Rev. E **61**, 1195 (2000).
[15] M. P. Allen and D. J. Tildesley, *Computer Simulation of Liquids* (Clarendon, Oxford, 1987).
[16] D. Frenkel and B. Smit, *Understanding Molecular Simulation* (Academic, San Diego, 1996).